REPORT DOCUMENTATION PAGE

Form Approved
OMB No. 0704-0188

1. AGENCY USE ONLY (Leave blank)	2. REPORT DATE	3. REPORT TYPE AND DATES COVERED
	April 11 1995	Performance Report: 2/21/94 – 2/20/95.

4. TITLE AND SUBTITLE

3D Vector Wavelet-based Subgrid Scale Model for LES of nonequilibrium turbulence

5. FUNDING NUMBERS

N00014–94–1–0510

6. AUTHOR(S)

Valery Zimin and Fazle Hussain

7. PERFORMING ORGANIZATION NAME(S) AND ADDRESS(ES)

Institute for Fluid Dynamics and Turbulence
University of Houston
4800 Calhoun
Houston Tx 77204-4792

8. PERFORMING ORGANIZATION REPORT NUMBER

9. SPONSORING/MONITORING AGENCY NAME(S) AND ADDRESS(ES)

Scientific officer Code: 332FD
Lawrence P. Purtell
Office of Naval Research
Baliston Tower One
800 North Quincy Street
Arlington, Virginia 22217-5660

10. SPONSORING/MONITORING AGENCY REPORT NUMBER

11. SUPPLEMENTARY NOTES

Assisted by Arindam Ghosh

12a. DISTRIBUTION/AVAILABILITY STATEMENT

12b. DISTRIBUTION CODE

13. ABSTRACT (*Maximum 200 words*)

We have laid the foundation to develop and validate LES using wavelets as a functional basis and based on subgrid scale (SGS) modeling using vector wavelets. Wavelet LES (WLES) consists of subgrid-scale model equations (SSM) and space-resolved model (SRM) equations . Using a vector wavelet decomposition of the velocity field a simple model for locally isotropic turbulence has been derived from the Navier-Stokes equation. This model, which involves no empirical or *adhoc* parameter, incorporates nonlocal inter-scale interactions, reveals backscatter and can be applied to represent small-scale turbulence in LES schemes. Stationary solutions of the model equations produce the Kolmogorov $k^{-5/3}$ inertial spectrum and the k^4 infra-red spectrum. We have completed derivation of the SRM equations based on the helical wave decomposition. We will test the SRM equations using the computational resources in this NAS operational year. A wavelet-based subgrid-scale model (WSSM) will be generalized to account for anisotropic and inhomogeneous turbulence in wall-bounded flows and will employ a nonuniform grid to resolve the near-wall structures.

14. SUBJECT TERMS			15. NUMBER OF PAGES 31
			16. PRICE CODE
17. SECURITY CLASSIFICATION OF REPORT	18. SECURITY CLASSIFICATION OF THIS PAGE	19. SECURITY CLASSIFICATION OF ABSTRACT	20. LIMITATION OF ABSTRAC

GENERAL INSTRUCTIONS FOR COMPLETING SF 298

The Report Documentation Page (RDP) is used in announcing and cataloging reports. It is important that this information be consistent with the rest of the report, particularly the cover and title page. Instructions for filling in each block of the form follow. It is important to *stay within the lines* to meet *optical scanning requirements*.

Block 1. Agency Use Only *(Leave blank)*.

Block 2. Report Date. Full publication date including day, month, and year, if available (e.g. 1 Jan 88). Must cite at least the year.

Block 3. Type of Report and Dates Covered. State whether report is interim, final, etc. If applicable, enter inclusive report dates (e.g. 10 Jun 87 - 30 Jun 88).

Block 4. Title and Subtitle. A title is taken from the part of the report that provides the most meaningful and complete information. When a report is prepared in more than one volume, repeat the primary title, add volume number, and include subtitle for the specific volume. On classified documents enter the title classification in parentheses.

Block 5. Funding Numbers. To include contract and grant numbers; may include program element number(s), project number(s), task number(s), and work unit number(s). Use the following labels:

C	- Contract	PR	- Project
G	- Grant	TA	- Task
PE	- Program Element	WU	- Work Unit Accession No.

Block 6. Author(s). Name(s) of person(s) responsible for writing the report, performing the research, or credited with the content of the report. If editor or compiler, this should follow the name(s).

Block 7. Performing Organization Name(s) and Address(es). Self-explanatory.

Block 8. Performing Organization Report Number. Enter the unique alphanumeric report number(s) assigned by the organization performing the report.

Block 9. Sponsoring/Monitoring Agency Name(s) and Address(es). Self-explanatory.

Block 10. Sponsoring/Monitoring Agency Report Number. *(If known)*

Block 11. Supplementary Notes. Enter information not included elsewhere such as: Prepared in cooperation with...; Trans. of...; To be published in.... When a report is revised, include a statement whether the new report supersedes or supplements the older report.

Block 12a. Distribution/Availability Statement. Denotes public availability or limitations. Cite any availability to the public. Enter additional limitations or special markings in all capitals (e.g. NOFORN, REL, ITAR).

DOD	- See DoDD 5230.24, "Distribution Statements on Technical Documents."
DOE	- See authorities.
NASA	- See Handbook NHB 2200.2.
NTIS	- Leave blank.

Block 12b. Distribution Code.

DOD	- Leave blank.
DOE	- Enter DOE distribution categories from the Standard Distribution for Unclassified Scientific and Technical Reports.
NASA	- Leave blank.
NTIS	- Leave blank.

Block 13. Abstract. Include a brief *(Maximum 200 words)* factual summary of the most significant information contained in the report.

Block 14. Subject Terms. Keywords or phrases identifying major subjects in the report.

Block 15. Number of Pages. Enter the total number of pages.

Block 16. Price Code. Enter appropriate price code *(NTIS only)*.

Blocks 17. - 19. Security Classifications. Self-explanatory. Enter U.S. Security Classification in accordance with U.S. Security Regulations (i.e., UNCLASSIFIED). If form contains classified information, stamp classification on the top and bottom of the page.

Block 20. Limitation of Abstract. This block must be completed to assign a limitation to the abstract. Enter either UL (unlimited) or SAR (same as report). An entry in this block is necessary if the abstract is to be limited. If blank, the abstract is assumed to be unlimited.

End-of-the Fiscal-Year Summary Report for 1995

Contract Information
Account Number 1–5–52704
Contract/Grant Title:
3D Vector Wavelet-Based Subgrid-Scale Model for LES of Nonequilibrium Turbulence
Sponsor: U.S.Navy Office of Naval Research
Sponsor I.D.: N00014-94-1-0510
Scientific officer: Lawrence P. Purtell
Principal Investigator:
Prof. Fazle Hussain
Dr. Valery Zimin
Mailing address: University of Houston Mechanical Engineering Dept. 77204-4792
Phone number: (713) 743-4545
Fax number: (713) 743-4544
E-Mail address: mece1w@jetson.uh.edu

A. Description of the Scientific Research Goals

The first objective of this research is to develop and validate a novel approach to subgrid scale modeling based on vector wavelets. This approach must be capable of treating non-equilibrium turbulence. The second objective is to develop a LES scheme, which uses wavelet-type helical basis functions for the space resolved scales, to describe anisotropic and wall-bounded flows. The third objective is to integrate the wavelet SSM in this new LES scheme. After developing this wavelet LES the next objective is to carry out LES of some nonequilibrium flows which will lead to a general purpose LES scheme capable of providing improved estimates of dynamical characteristics such as skin friction and mixing, as well as enabling prediction and adaptive control of separation in turbulent boundary layers of naval interest.

B. Significant Results in the Past Year

B1. Introduction

We have laid the foundation to develop and validate LES using wavelets as a functional basis and based on subgrid scale (SGS) modeling using vector wavelets. Wavelet LES (WLES) consists of subgrid-scale model equations (SSM) and space-resolved model (SRM) equations . Using a vector wavelet decomposition of the velocity field a simple model for locally isotropic turbulence has been derived from the Navier-Stokes equation. This model, which involves no empirical or *adhoc* parameter, incorporates nonlocal inter-scale interactions, reveals backscatter and can be applied to represent small-scale turbulence in LES schemes. Stationary solutions of the model equations produce the Kolmogorov $k^{-5/3}$ inertial spectrum and the k^4 infra-red spectrum. We have completed derivation of the SRM equations based on the helical wave decomposition. We will test the SRM equations using the computational resources in this NAS operational year. A wavelet-based subgrid-scale model (WSSM) will be generalized to account for anisotropic and inhomogeneous turbulence in wall-bounded flows and will employ a nonuniform grid to resolve the near-wall structures.

B2. LES Scheme

In WLES we start by representing the flow field using regularly distributed fixed helical basis functions in physical space. These fixed basis functions correspond to the macroscopic (resolved) scale in conventional LES. Then, in each grid box, we consider a hierarchy of small-scale wavelets corresponding to the subgrid scales (SGS's). Our SSM equations are derived directly from the incompressible Navier-Stokes equations by a Galerkin projection onto a complete wavelet basis. Through analytical approximations (thereby eliminating calibration constants) to the wavelet interaction

coefficients, a system of ODE's is obtained. These ODE's describe the energy contained in wavelets of scales ℓ, $\ell/2$, $\ell/4$,..., $\ell/2^{L-1}$, where L is the number of levels in the SGS wavelet hierarchy. These L variables enable the energy spectrum to evolve dynamically and thus make the SSM ideally suited for nonequilibrium flows. We have reproduced crucial features of homogeneous turbulence using this model: *e.g.* k^4 infra-red spectrum, the value of Kolmogorov constant (1.48), conservation of equilibrium k^2 spectrum, self-similar decay of stationary spectrum (with the correct decay rate) etc. The results from our model are compared with recent experimental[1] and numerical[2] results. Currently we are testing the model for nonequilibrium situations. We are also deriving a new SSM based on the helical wave decomposition.

For the WLES scheme, we use macroscopic scales resolved on Eulerian grid points (N in number) while the residual scales are modeled using wavelets which act as a crucial dynamical link between macroscopic and residual scales. This feature is particularly suited for nonequilibrium flows, since SGS wavelets mimic the physical nature of turbulence and allow accurate modeling of significant spatial and temporal variations in turbulence intensity. A notable feature of this scheme is that most of the variables are used to describe the SGS dynamics (namely, L SGS variables for each grid point); this is in contrast to conventional SGS models, which have no parameters for describing the dynamics.

In brief, the scheme can be represented in the following way; we start by decomposing the velocity field in terms of the wavelet basis:

$$u = \sum A_\alpha v_\alpha ,$$

where v_α is the wavelet corresponding to the index α and $\alpha = (N,\nu,\mathbf{m})$ is a composite index. N represents the scale, ν is the helicity index, and $\mathbf{m}$ is the location of the center of the wavelet. A_α represents the amplitude of the wavelets used to

decompose the velocity field. Note that N = 0 represents the resolved scales, the level at which boundary conditions are specified. To decompose velocity field at the resolved scales, we employ a pair of helical basis functions. The evolution equation for the wavelet amplitude can be written as

$$\frac{dA_\alpha}{dt} = L_\alpha (A_\beta)$$

The nonlinear operator L consists of the inviscid and the viscous part. The complete evolution equation can be written as:

$$\sum_{\mu m} P_{Nv\eta\mu m} \dot{A}_{N\mu m} = \sum_{M\mu m} \sum_{L\lambda l} T_{Nv\eta M\mu m L\lambda l} A_{M\mu m} A_{L\lambda l} + \sum_{\mu m} K_{Nv\eta\mu m} A_{N\mu m}.$$

This equation will be explained in detail in §B5.

The accuracy of the scheme depends on the truncation procedure adopted to calculate the coefficients T and K which correspond to the inviscid and the viscid part respectively. The influence of a given wavelet decays rapidly as we move away from its center. The truncation procedure is based on a threshold approximation which retains all the coefficients lesser than a specified value. For the subgrid scales, the interaction coefficients are assumed to be 1 if a triad of wavelets overlap and are set to zero if otherwise. All calculations are carried out in the coefficient space. WSSM has no arbitrary constants and thus does not rely on experiments for empirical data.

B3.Differences with the traditional LES

Currently popular LES methods do not track the evolution of small-scale turbulence and thus assume that at each instant the subgrid turbulence is in statistical equilibrium with the large-scale motion. This implies that all scales within the nonstationary part of the spectrum must be modeled as large-scale. If a subgrid model would involve variables and equations for describing small-scale turbulence evolution, the assumption of statistical equilibrium between large and small scales would no longer be required, and modeling of only the energy containing (inhomogeneous) largescales would be sufficient. This will significantly reduce the cut-off spatial frequency for the large scales, thereby decreasing the operation count of the LES drastically. WLES employs just such a model using a vector wavelet approach to small-scale turbulence model.

Another significant feature of the WLES is that it does not have a sudden loss of resolution. In the traditional LES schemes above the cut-off wave number suddenly we have only a statistical description of the flow; this accentuates the predictability problem of the LES drastically. In WLES below the cut-off wave number we solve a simplified ODE version of the NSE thus preserving a model dynamical description of the flow. This method is inherently consistent with the fact that there is no spectral gap between large scale structures necessary for the existence of turbulence and the secondary eddies generated from them . In this scheme it is very easy to satisfy the "stringent"[3] requirement that the low frequency part of the spectra not be affected by the procedure used to remove unwanted degrees of freedom from the dynamical description of the flow. Moreover this approach is amenable to construction of models for production process as the wavelets closely parralel the actual eddies.

B4 Importance of the model equations

Derivation and testing of the model equations for WSSM is a central part of this work because it is these model equations which enable the WLES to track the dynamical evolution. However, it is of utmost importance to note that in the process we also have a simplified ODE version of the NSE which can accurately describe turbulence. Discovery of these equations may have far-ranging implications for turbulence modeling beyond the confines of the narrow context of this particular LES development.

Normally turbulence is treated without taking helicity explicitly into account; however, recently it has been shown that description of turbulence in terms of two helical basis functions is conducive to a better physical understanding. In the framework of WLES the use of helical basis functions allows us to conserve two integral constraints: energy and helicity.

B5. Deriving the model equations

To obtain a finite dimensional approximation of NSE, we use the method of weighted residuals with wavelet based trial function,

$$\mathbf{u}(x,t) = \sum_{Nvn} A_{Nvn}(t)\mathbf{v}_{Nvn}(\mathbf{x}). \tag{1}$$

The divergence-free vector wavelets $\mathbf{v}_{Nvn}$ are defined as

$$\mathbf{v}_{Nvn}(\mathbf{x}) = -\frac{\pi}{2}\rho_N^{-1/2}\,\mathbf{e}_v \times \nabla_{\mathbf{s}}\left(\frac{\cos(s)-\cos(2s)}{s^2}\right) \tag{2}$$

Here

$$\rho_N = (7\pi/9)\,2^{3N}; \qquad \mathbf{s} = \pi 2^N(\mathbf{x}-\mathbf{x}_{Nn}). \tag{3}$$

The index N denotes the scale of the wavelet. Fourier transforms of wavelets are localized inside spherical shells in the wavenumber space $\{\pi 2^N < k < \pi 2^{N+1}\}$. Each

wavelet can be considered as an axisymmetric vortex with its axis along one of the unit vectors $\hat{\mathbf{e}}_\nu$ (Fig. 1). The wavelet centers $\mathbf{x}_{Nn}$ are randomly distributed in the physical space with a density ρ_N, which is chosen to produce a uniform approximation of the velocity field in the N-th wavenumber shell. The vorticity magnitude of each vortex of the scale N is significant only in a spherical region of radius $\rho_N^{-1/3}$ with the center located at $\mathbf{x}_{Nn}$. We choose ρ_N^{-3} as the volume of the wavelet localization region in the physical space.

The Galerkin projection of NSE on the basis (2) has a form

$$\sum_{\mu m} P_{N\nu n\mu m} \dot{A}_{N\mu m} = \sum_{M\mu m} \sum_{L\lambda l} T_{N\nu nM\mu mL\lambda l} A_{M\mu m} A_{L\lambda l} + \sum_{\mu m} K_{N\nu n\mu m} A_{N\mu m}, \tag{4}$$

where

$$P_{N\nu n\mu m} = \int d^3x \left\{ \mathbf{v}_{N\nu n} \cdot \mathbf{v}_{N\mu m} \right\}, \tag{5}$$

$$T_{N\nu nM\mu mL\lambda l} = \frac{1}{2} \int d^3x \left\{ \mathbf{v}_{N\nu n} (\mathbf{v}_{M\mu m} \nabla) \mathbf{v}_{L\lambda l} + \mathbf{v}_{N\nu n} (\mathbf{v}_{L\lambda l} \nabla) \mathbf{v}_{M\mu m} \right\}, \tag{6}$$

$$\text{and } K_{N\nu n\mu m} = \int d^3x \left\{ \mathbf{v}_{N\nu n} \cdot \Delta \mathbf{v}_{N\mu m} \right\}. \tag{7}$$

The matrix elements $T_{N\nu nM\mu mL\lambda l}$ describe the nonlinear interactions between $\mathbf{v}_{N\nu n}$, $\mathbf{v}_{M\mu m}$, and $\mathbf{v}_{L\lambda l}$. Consequently, they have significant values only if the localization regions of the individual wavelets forming this triad overlap in physical space. These elements scale with the wavelet scale as

$$T_{(N+P)\nu n(M+P)\mu m(L+P)\lambda l} = 2^{5P/2} T_{N\nu nM\mu mL\lambda l}. \tag{8}$$

Conservation of kinetic energy (due to the nonlinear terms in equation (4)) is guaranteed by the following property of the matrix **T**

$$T_{NvnM\mu mL\lambda l} + T_{M\mu mL\lambda lNvn} + T_{L\lambda lNvnM\mu m} = 0. \tag{9}$$

We represent the wavelet amplitudes as

$$A_{Nvn}(t) = A_N(t)\, a_{Nvn}(t), \tag{10}$$

where the new variables A_N, later called the shell variables, are linked to the kinetic energy $E_N(t)$ in the N-th wavenumber shell as

$$E_N(t) = \frac{1}{2}\rho_N A_N^2(t). \tag{11}$$

Taking an ensemble average over the realizations with the same $A_N(t)$ we obtain the following exact equations for A_N from (4), (10), and (11)

$$\dot{A}_N = \sum_{ML} \Phi_{NML} A_M A_L + \Lambda_N A_N, \tag{12}$$

where

$$\Phi_{NML} = \rho_N^{-1} h^{-3} \sum_{\nu\mu\lambda} \sum_{nml} T_{NvnM\mu mL\lambda l} \langle a_{Nvn} a_{M\mu m} a_{L\lambda l} \rangle, \tag{13}$$

and

$$\Lambda_N = \rho_N^{-1} h^{-3} \sum_{\nu\mu} \sum_{nm} K_{Nvn\mu m} \langle a_{Nvn} a_{N\mu m} \rangle. \tag{14}$$

Here <> denotes the statistical ensemble average over all possible realizations of the phase variable: $a_{Nvn}(t)$.

To obtain the model equations for A_N we introduce the following closure correlations

$$\langle a_{Nvn} a_{M\mu m} a_{L\lambda l} \rangle = \langle a^2_{Nvn} \rangle^{1/2} \langle a^2_{M\mu m} \rangle^{1/2} \langle a^2_{L\lambda l} \rangle^{1/2}$$

$$(Q_{NML} T_{NvnM\mu mL\lambda l} + Q_{MLN} T_{M\mu mL\lambda lNvn} + Q_{LNM} T_{L\lambda lNvnM\mu m}), \qquad (15)$$

where

$$Q_{NML} = 2^{-5N/2} Z^{-1/2}_{NML}, \qquad (16)$$

and Z_{NML} is the number of the overlapping wavelet triads that include the wavelet v_{Nvn} as one of the interacting wavelets. Note that $\langle a_{Nvn} a_{M\mu m} a_{L\lambda l} \rangle$ is scale invariant due to the first multiplier in (16), while $Z^{-1/2}_{NML}$ accounts for the resulting interaction between the wavelet v_{Nvn} and Z_{NML} pairs of wavelet, which have localization regions overlapping with the localization region of v_{Nvn}. In addition, we neglect the cross-correlations of the normalized wavelet amplitudes inside the shells

$$\langle a_{Nvn} a_{N\mu m} \rangle = \frac{1}{3} \delta_{v\mu} \delta_{nm} \qquad (17)$$

The factor 1/3 follows from (10) and (12). This assumption is necessary only to simplify calculations of K and is justified because the value of nondiagonal elements are much less than the diagonal elements.

For a random distribution of the vortex centers the sums in (12) were calculated analytically. The signs of Φ_{NML} are uniquely determined by energy conservation in the limit of zero viscosity. The diagonal interaction coefficients (*i.e.* when two of the three indices are equal) Φ_{NMM}, Φ_{NMN}, and Φ_{NNL} have significantly higher values than the

adjacent nondiagonal elements. To simplify the model equations and make them amenable to analytical investigation we first neglect the nondiagonal coefficients Φ_{NML} and then approximate the diagonal coefficients by exponential functions. This leads to the following system of model equations

$$\dot{A}_N = 2^{5N/2} \sum_M B_M \left[2^{-4M} A_N A_{N-M} - 2^{3M/2} A_{N+M}^2 \right] - 2^{2N} D A_N, \qquad (18)$$

where $B_{M<-1} = 0$; $B_{-1} = 0.387$; $B_0 = 0$; $B_{M\geq 1} = 2.19$; $D = 93\pi^2/35$. Note that all these parameters are analytically calculated and not empirically determined. We choose the length, velocity and time scales to be $l_0 = \rho_0^{-1/3}$, l_0^2/ν and ν/l_0 respectively, where ν is the kinematic viscosity. In these units it is convenient to consider Reynolds number for each scale $Re_N = A_0 2^{N/2}$.

At zero viscosity (the same as putting D = 0) the equations (18) conserve the total kinetic energy $E = \sum E_N$ and has the exact stationary solution

$$A_N = 0.557\varepsilon^{1/3} 2^{-11N/6}, \qquad (19)$$

which corresponds to the Kolmogorov energy spectrum $E(k) = 1.47\varepsilon^{2/3}k^{-5/3}$. If the energy is initially confined in only one shell, e.g. at t=0, $A_N = 0$ only if $N \neq 0$, then small disturbances δA_N grow as $\dot{\delta A}_N = 2.19 \cdot 2^N A_0^2$. This analytical result corresponds to the elevation of the k^4 infra-red spectrum, which is simultaneously generated at all scales.

It is to be noted that the closure relation (15) was derived later. Initial derivation of the equation (18) followed dynamical assumptions to approximate the interaction coefficients. The approximation procedure for these interaction coefficients is presented in the appendix 1.

B6 Results from the model set of eqiuations

Solutions of (18) were obtained numerically for viscous cases by a variable coefficient ODE solver[4] with a pre-conditioned Krylov subspace iterative method[5]. The most significant result so far is presented in the Fig 2. The initial energy was confined in the shell N = 0 and the initial R_λ ($Re_{N=0}$) was 10^5. The solutions display a k^4 infrared spectrum to the left of the initial energy containing scale and $k^{-5/3}$ Kolmogorov inertial spectrum to the right. Thus both the energy transfer from the small scale to the large scale (backscatter) and the large scale to the small scale (cascade) can be adequately captured by the simple model. The evolution is shown from 0.1 to 1 (in steps of 0.1) eddy turnover time. In the dissipative range the energy spectrum decays as $\exp(-\beta\eta k)$ with $\beta = 5.37$, which is close to $\beta=5.2$ reported recently by Saddoughi and Veeravalli[1] for a large Re boundary layer(Re_θ = 74000; R_λ = 600). The continuous spectrum was obtained by a cubic-spline interpolation of the energy spectrum corresponding to the shell variables. Our results are compared with the time evolution of the kinetic-energy spectrum in an unforced pseudo-spectral 128^3 large-eddy simulation by Lesieur and Rogallo[2], started initially with a k^8 spectrum at low k. The point to note here is that the wavelet based model equations capture the infra-red spectrum with the same accuracy as an LES where the eddy viscosity was evaluated using EDQNM kinetic energy transfer. However, our simulations cover a much wider range of scales (6 decades compared with 2 decades in the LES) and also include the dissipation range. A detailed comparison between the LES results and ours is beyond the scope of this letter. Note that this evolution is tracked by using only 32 shell variables compared with 128^3 variables in the LES.

Thus we have developed a successful model for the small scale turbulence dynamics involving simple ordinary differential equations which are much simpler

than the EDQNM model (only one known to represent backscatter accurately) and thus have a good chance of being successfull as a subgrid model. More importantly, since these equations can track the small-scale evolution using very few shell variables and no adhoc parameters, they can be used to model nonequlibrium turbulence.

The growth and decay of the shell variables are shown in the figure 3. It is to be noted that the there is a delay time before the amplitudes start growing which increases as the wavenumber increases. This delay represents the time required for the energy to cascade down to smaller scales. After an initial rise in the amplitudes the value of the shell variables settle down to the value of the Kolmogorov constant. As the wavenumbers grow the effect of viscosity becomes more and more pronounced in lowering the equilibrium value.

The value of Kolmogorov constant was estimated from the rate of energy estimate into the system. The spectrum is given by $E(k) = C\varepsilon^{2/3}k^{-5/3}$, while it can be shown that the energy of the n-th shell: $E_N \sim 4.721\varepsilon^{2/3}A_o^{\ 2}$. From these two relations Kolmogorov constant was estimated to be 1.48.

In figure 4 we observe the free-decay of turbulence when the forcing is withdrawn. The spectrum retains the self-similarity as expected. The rate of energy decay was proportional to t^{-2}.

In figure 5 we observe the conservation of an initial k^2 energy spectrum to the left of the energy-containing wavenumber. This is a further test to observe if the behavior of the equations closely parallel the behavior of turbulence. The k^2 energy spectrum correspond to the situation when the energy is equally divided among all scales and hence this is a situation where there is no flow of energy into these scales. This feature was correctly captured by the model equations.

In figure 6 we test the behavior of the equations under a simple case of nonequilibrium turbulence where we add a periodic driving force. We observe that the flux to the large scale is quite different from the flux to the small scales while the dissipation is essentially constant. This demonstrates the capability of the model to handle non-equilibrium situation. This extension to non-axisymmetry will be the primary focus of our efforts next year.

B7 Extension to helical models: gateway to anisotropic and inhomogenous flows

To derive a helical version of the WSSM it is not advisable to proceed directly by using wavelet basis functions. It is better to work first with a helical Fourier representation of the Navier Stokes equation and then introduce wavelets. This not only makes the analytical calculations tractable but also allows us to generalize the WSSM to inhomogeneous helical turbulence with random anisotropy. This development of an explicit helical Fourier representation of NSE is succinctly sketched below.

In the helical Fourier representation the equations are equivalent to the original NSE, however they describe the motion of the fluid in terms of four scalar functions: the amplitudes $A_\alpha(\mathbf{k},t)$ and phases $\Phi_\alpha(\mathbf{k},t)$ of the right handed ($\alpha = +1$) and the left handed ($\alpha = -1$) helical Fourier modes. It is possible to express the spectral densities of kinetic energy E and helicity using $A_\alpha(\mathbf{k},t)$ alone.

$$E(\mathbf{k},t) = \frac{1}{2}\sum_\alpha A_\alpha^2(\mathbf{k},t); \qquad H(\mathbf{k},t) = \sum_\alpha \alpha k A_\alpha^2(\mathbf{k},t).$$

Thus both fundamental quantities E and H have diagonal form in this representation.

The equations for the amplitudes and phases of the helical Fourier modes follow.

$$(\partial_t + k^2)A_\alpha(\mathbf{k},t) =$$

$$= \sum_{\beta} \sum_{\gamma} \int d^3q \; M_{\alpha\beta\gamma}(k,q,p) \cos[\Theta_{\alpha\beta\gamma}(k,q,p) - \Phi_{\alpha}(k,t) - \Phi_{\beta}(q,t) - \Phi_{\gamma}(p,t)] A_{\beta}(q,t) \, A_{\gamma}(p,t).$$

$$A_{\alpha}(k,t) \partial_t \, \Phi_{\alpha}(k,t) =$$

$$= \sum_{\beta} \sum_{\gamma} \int d^3q \; M_{\alpha\beta\gamma}(k,q,p) \sin[\Theta_{\alpha\beta\gamma}(k,q,p) - \Phi_{\alpha}(k,t) - \Phi_{\beta}(q,t) - \Phi_{\gamma}(p,t)] A_{\beta}(q,t) \, A_{\gamma}(p,t),$$

where $M_{\alpha\beta\gamma}(k,q,p)$ and $\Theta_{\alpha\beta\gamma}(k,q,p)$ represent the amplitude and the phase of the kernel of the integral operator describing the interactions of the triads of helical Fourier modes.

The next step is to derive a closure procedure for the helical equations independent of the wavelet formalism. Then it will be very easy to extend this scheme to anisotropic and inhomogeneous flows.

B8. Conclusions

We have developed a successful model for the small scale turbulence dynamics involving simple ordinary differential equations which are much simpler than the EDQNM model (only one known to represent backscatter accurately) and thus have a good chance of being successfull as a subgrid model. More importantly, since these equations can track the small-scale evolution using very few shell variables and no adhoc parameters, they can be used to model nonequlibrium turbulence.

The preliminary WSSM based on energy amplitudes predict the energy spectrum quite accurately. Thus, it is worthwhile to extend this WSSM based only on energy amplitudes to non-equilibrium situations, while continuing to develop helical WSSM which uses both energy and helicity amplitudes. Since the WSSM that uses only energy amplitude is much simpler than the helical SSM the use of it will be justifiable if it can deliver comparable performance to helical WSSM even if the domain of its applicability

turn out to be somewhat restricted. Moreover the development of only energy based WSSM will provide important guidelines and checkpoints for the helical WSSM.

Direct attempts to derive helical WSSM require extremely lengthy analytical calculations; unfortunately these calculations are not amenable to solutions via standard analytical softwares either. Hence the process was divided into three parts: i) derivation of NSE in the Fourier space using energy and helicity amplitudes ii) implementation of a closure procedure and iii) introduction of wavelet basis. Derivation of the equations are complete and rest of the work is in progress. Since the closure procedure is introduced prior to the introduction of wavelet generalization to anisotropic and inhomogeneous turbulence becomes simpler to achieve.

Appendix

A1. Calculation of R coefficients

$$v_{Nvn}(x) = \int V_{Nvn}(k')\, e^{2\pi i\, k'\bullet x}\, dk'$$

$$v_{M\mu m}(x) = \int V_{M\mu m}(k'')\, e^{2\pi i\, k''\bullet x}\, dk''$$

$$v_{L\lambda l}(x) = \int V_{L\lambda l}(k''')\, e^{2\pi i\, k'''\bullet x}\, dk'''$$

Using the above relations

$$K_{NvnM\mu m} = \int V^{*}_{Nvni}(k)(2\pi i k_j)^2 V_{M\mu mi}(k) = \frac{93\pi^2}{35} = 26.2$$

$$R_{NvnM\mu mL\lambda L} = \int dx \int dk') \int dk'') \int dk''' \left(\frac{3i}{\sqrt{7\pi}}\right)^3 2^{\frac{-3}{2}(N+M+L)} \frac{(k'\times e_\nu)_i}{|k'|} \frac{(k''\times e_\nu)_j}{|k''|}$$

$$2\pi i k''' \frac{(k'''\times e_\nu)_i}{|k'''|} e^{-2\pi i\,(k'\bullet x_{Nn} + k''\bullet x_{Mm} + k'''\bullet x_{Ll'} - k'\bullet x - k''\bullet x + k'''\bullet x)}$$

The exponential part can be rewritten as

$$e^{-2\pi i\,(k'\bullet x_{Nn} + k''\bullet x_{Mm} + k'''\bullet x_{Ll'} - (k'+k''+k''')\bullet x)}$$

Since **x** appears only in the exponential we integrate over **x** first.

Now $e^{-2\pi i(\mathbf{k}'+\mathbf{k}''+\mathbf{k}''')\bullet\mathbf{x}} = \delta(\mathbf{k}'+\mathbf{k}''+\mathbf{k}''')$.

Hence the integral exists only if $\mathbf{k}'+\mathbf{k}''+\mathbf{k}''' = 0 \Rightarrow \mathbf{k}''' = -\mathbf{k}'-\mathbf{k}''$

Changing notation,

$\mathbf{k}' \equiv \mathbf{k}$ and $\mathbf{k}''' \equiv \mathbf{k}' \Rightarrow \mathbf{k}'' \equiv -\mathbf{k}'-\mathbf{k}$.

Thus the structure of the R matrix is

$$\mathbf{R}_{\mathrm{NvnM\mu mL\lambda L}} = \int d\mathbf{k}' \int d\mathbf{k}'' \left\{ \mathbf{V}_{\mathrm{Nvni}}(\mathbf{k})\mathbf{V}_{\mathrm{M\mu mj}}(-\mathbf{k}'-\mathbf{k})\, 2\pi i\, \mathbf{k}'\, \mathbf{V}_{\mathrm{L\lambda li}}(-\mathbf{k}') \right\}.$$

Now we proceed to obtain the model equations by replacing the exact expressions for the interaction coefficients, with a threshold approximation. The approximation is equivalent to stating that the modelled R is equal to the rms value of exact R when three wavelets overlap and 0 when they do not.

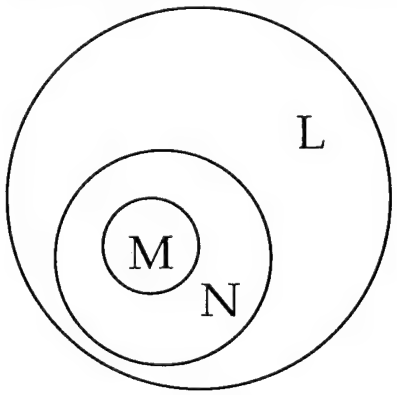

Overlapping wavelet triads

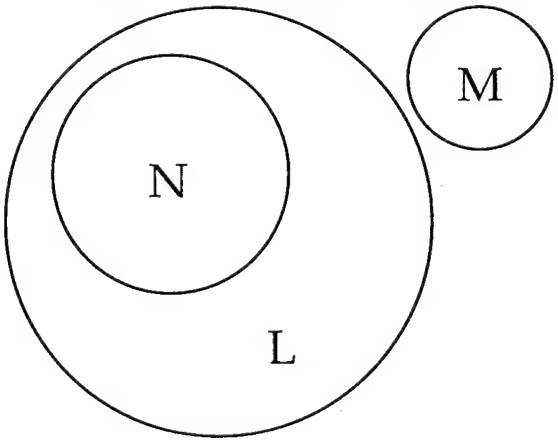

Non overlapping wavelet triad

For some fixed levels N,M,L we estimate by integrating over all possible configurations of x_{Nn} , x_{Mm} , x_{Ll}.

$$R^2_{NML} = \frac{W}{27}\sum_{\nu\mu\lambda} \int dx_{Mm} \int dx_{Ll} R^2_{N\nu nM\mu mL\lambda l}$$

This involves 18 integrations: 3 for dx_{Mm}, 3 for x_{Ll} 6 + 6 for each **R** in $\mathbf{R}^2$, and 27 summations over ν, μ and λ.

Actual distribution of R is complex so it is approximated by a step function, *i.e.* if all three wavelets (N,M,L) overlap in some region **R** has some constant value; else, it is zero.

This yields $W = \left(\frac{7\pi}{9}\right)^2 2^{3q}$

$q = M+L-N,\ M<N,\ L<N$

$q = M-N,\ M< N,\ L\geq N$

Thus a step approximation of **R** as described above yields the scaling law $k^{-(5/3)}$.

A more accurate approximation of **R** in the mean square sense yields $k^{-(5/3)+\chi}$.

χ is a small correction. In the above estimate of **R** the sign of **R** is ambiguous.

By substituting the expressions for basis functions and proceeding as before it can be shown that

$$\sum_{\nu\mu\lambda} \int \int R^2_{N\nu nM\mu mL\lambda l} dx_{Mm}\, dx_{Ll} = \frac{4.27^2}{\pi.7^3} 2^{-3(N+M+L)} \int dk dk' \left\{ \frac{k^2 k'^2 (1+\cos^2\theta)\sin^2\theta}{k^2+k'^2-2kk'\cos\theta} \right\}$$

Thus,

$$R^2_{NML} = \frac{4\pi}{21} 2^{-3(N+M+L-q)} \int dk dk' \left\{ \frac{k^2 k'^2 (1+\cos^2\theta)\sin^2\theta}{k^2+k'^2-2kk'\cos\theta} \right\}$$

Point to note:

We can write $T_{NML} = \frac{1}{2}(R_{NML} + R_{NLM})$.

This will make the coefficient matrix symmetric.

However, in this case,

$$T^2_{NML} = \frac{1}{4}R^2_{NML} + \frac{1}{2}R_{NML}R_{NLM} + \frac{1}{4}R^2_{NLM}$$

Thus we need to evaluate the cross terms, which can be done in the following manner:

$$\sum_{\nu\mu\lambda} \int\int R_{N\nu nM\mu mL\lambda l} R_{N\nu nM\mu mL\lambda l}\, dx_{Mm}\, dx_{Ll} =$$

$$\frac{32.27^2\pi}{7^3} 2^{-3(N+M+L)} \int d\vec{k}\, d\vec{k'} \left\{ \frac{k^4 k'^3 (k - k'\cos\theta)\sin^3\theta\cos\theta}{k^2 + k'^2 - 2kk'\cos\theta} \right\}$$

$$2^{N-1} < k < 2^N$$

$$2^{L-1} < k < 2^L$$

$$2^{M-1} < \sqrt{k^2 + k'^2 - 2kk'\cos\theta} < 2^M$$

Based on approximations of T_{NML} we can arrive at the model equation

$$\dot{A}_N = \sum_{M\neq 0} T_{NM}(A^2_{N+M} - A_N A_{N-M}) - K_N A_N + F_N.$$

Using scaling arguments we get the equation in the form

$$\dot{A}_N = 2.19\, 2^{\frac{2}{3}N}[2^{\frac{-1}{3}}(A^2_{N-1} - A_N A_{N+1}) + \sum_{p=1}^{9} 2^{-\frac{13}{6}p}(A_N A_{N-p} - A^2_{N+p})] - 22.62^{2N} A_N.$$

Here p denotes the levels of interaction.

C. Plans for Next Year's Research

Our first objective is to further validate our wavelet LES scheme by comparing turbulence statistics with DNS data for turbulent boundary layers and a backward facing step, at low R_λ and at equilibrium. We are particularly interested in capturing

prominent features of these flows, such as the near-wall streak spacing and the boundary layer reattachment length for the backward facing step.

To evaluate the applicability of wavelet LES for studying flow physics in practical flows, we will investigate nonequilibrium effects such as strong inhomogeneity, pressure gradients and wall curvature. Results from wavelet LES for moderate R_λ will first be compared with those from other LES subgrid-scale models, followed by wavelet LES at R_λ unattainable by conventional schemes. These high R_λ results will be validated and compared with experiments on turbulent boundary layers to be carried out concurrently in our laboratory. Also, to investigate the performance of wavelet LES in bounded flows, we will simulate transition to fully developed turbulent pipe flow and an oscillating pipe flow and compare these results with available experimental data.

Validation of Wavelet LES. The wavelet LES will be validated by comparing with DNS of turbulent channel flow at Re = 3300[6] and DNS of flow over a backward facing step[7] at Re = 6000. For the backward facing step, we will run two cases corresponding to the low step (W/H = 2.5) and high step (W/H = 1.25), where H and W are respectively the step and channel heights.

Investigation of nonequilibrium effects. Wavelet LES can in principle be accurately applied to high R_λ, in the range $R_\lambda = 10^4$ to $R_\lambda = 10^5$. These high R_λ values will be used for experimental comparisons (data from turbulent boundary layer facility in our laboratory) and studies of fundamental turbulence physics; low to moderate R_λ are necessary for comparisons with DNS. First, we will consider fully developed turbulent boundary layer with periodic boundary conditions and an impulsively applied mean

spanwise pressure gradient to investigate inhomogeneity and high Re effects. We will then simulate a boundary layer with spanwise wall motion, for comparison with work in progress by Kim *et al.* [8]. To investigate the effects of wall curvature, we will consider a turbulent flow over a cylinder for $\gamma = 5$, where γ is the ratio of the boundary-layer thickness to cylinder radius. These results will be compared with the minimal flow DNS of Neves *et al.* [9]. To investigate resolution of separation and reattachment, we will perform LES of flow over a backward facing step for W/H = 1.25 (high step) and 2.5 (low step), with no-slip conditions on the solid wall.

LES of bounded flows. For comparison with experimental data, we will first carry out wavelet LES of transitioning pipe flow, for comparison with DNS and experiments by Eggels *et al.* [10]. The Reynolds number based on the centerline velocity and pipe diameter (Re_c) will be 7000 in this case. To evaluate our LES scheme under non-equilibrium conditions, we will consider an oscillating pipe flow with $Re_c \sim 10000$. Experimental data for this flow will be obtained from the existing pipe flow facility here at the University of Houston.

Extension to anisotropy and inhomogeneous flows

The first step in this direction will be to derive a closure procedure for the helical equations and compare the results from this closed helical SSM with the WSSM results. As the helical SSM introduces wavelets after the closure procedure it can easily be tailored to be applied to anisotropic and inhomogeneous flows.

Status compared to original milestones

Originally proposed: YEAR I	**Achieved: YEAR I**
Repeat tests of analytical and computational analysis of prior hierarchical SGS models.	A detailed analysis was done and a way of improving earlier models was found which led to a new model.
A priori testing of basic SGS model using DNS data from homogeneous turbulence and free shear flows.	A new SGS model was derived and tested.
Develop and validate the basic LES scheme for homogeneous turbulence: to be started in first year and completed in the second year.	The basic equations for LES has been derived and tested. The code will be developed and validated this year.
Originally proposed: YEAR II & III	**Plans: YEAR II**
Validate LES for wall-bounded flows against DNS	To be done (Details above)
Refine new SGS to handle anisotropy and SGS helicity	To be done (Details above)
Develop SGS for nonequilibrium turbulence	To be done (Details above)

D.References

[1] S.G. Saddoughi and S.V. Veeravalli, "Local isotropy in turbulent boundary layers at high Reynolds number," J. Fluid Mech. **268**, 333 (1994).

[2] M. Lesieur and R. Rogallo, "Large-eddy simulation of passive scaler diffusion in isotropic turbulence," Phys. Fluids A **1**, 718 (1989).

[3] S. Orszag, I. Staroselsky and V. Yakhot, "Some basic challenges for large eddy simulation research," in *Large Eddy Simulation of Complex Engineering and Geophysical Flows*, edited by B. Galperin and S. Orszag (Cambridge University Press, 1993), 55.

[4] P. Brown, G. Byrne, and A.Hindmarsh, "VODE: a variable coefficient ODE Solver," SIAM J. Sci. Stat. Comput. **10**, 1038 (1989)

[5] G. Byrne, "Pragmatic Experiments with Krylov methods in the stiff ODE setting," in *Computational Ordinary Differential Equations* , edited by J. Cash and I. Gladwell (Clarendon Press, Oxford, 1992), 323.

[6] J. Kim, P. Moin and R. Moser, "Turbulence statistics in fully developed channel flow at low Reynolds number," J. Fluid Mech. **177**, 133 (1987).

[7] A.S.Neto, D. Grand, O. Metais and M. Lesieur, J. Fluid Mech. **256**, 1 (1993).

[8] J. Kim, G.Coleman and A. Le, "The effect of mean streamwise vorticity on turbulent boundary layers" , Personal Communication (1994).

[9] J.C. Neves, P. Moin, and R.D. Moser, "Effects of convex transverse curvature on wall-bounded turbulence. Part 1. The velocity and vorticity," J. Fluid Mech. **272**, 349 (1994).

[10] Eggels, J., Unger, F., Weiss, M., Westerwell, J., Adrian, R., Friedrich, R. & Nieuwstadt, F. 1994, *J. Fluid Mech.* **268**, p 175.

E. List of Figures

F. List of Publications/Presentations

V.D. Zimin and F. Hussain, "Wavelet based model of small-scale turbulence", subnitted to Physics of Fluids.

V.D.Zimin, M.V. Melander, D.Virk and F. Hussain, "3-D Vector wavelet based subgrid scale model for LES," ONR Workshop on nonequilibrium turbulence, Palo Alto (1994).

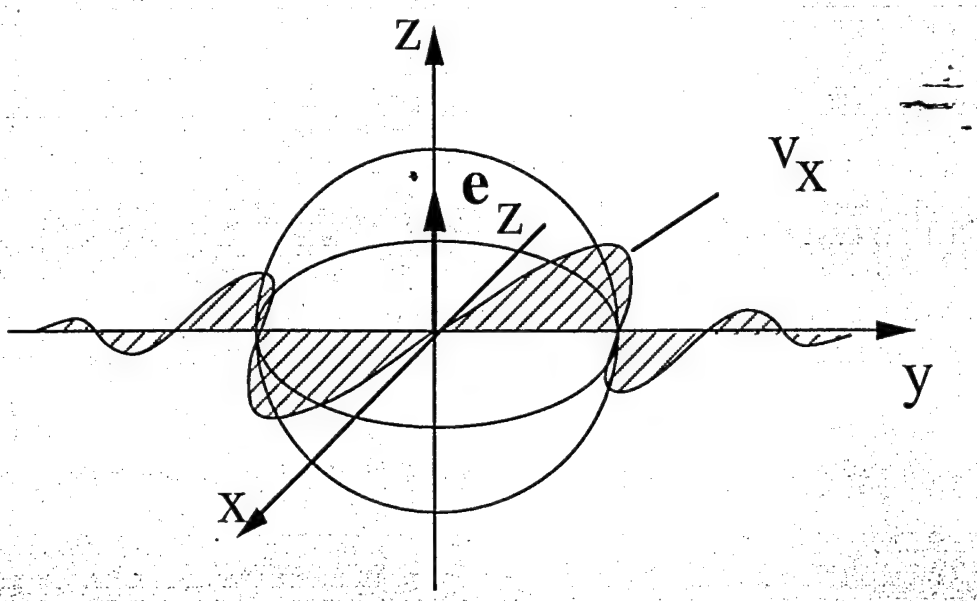

Figure 1

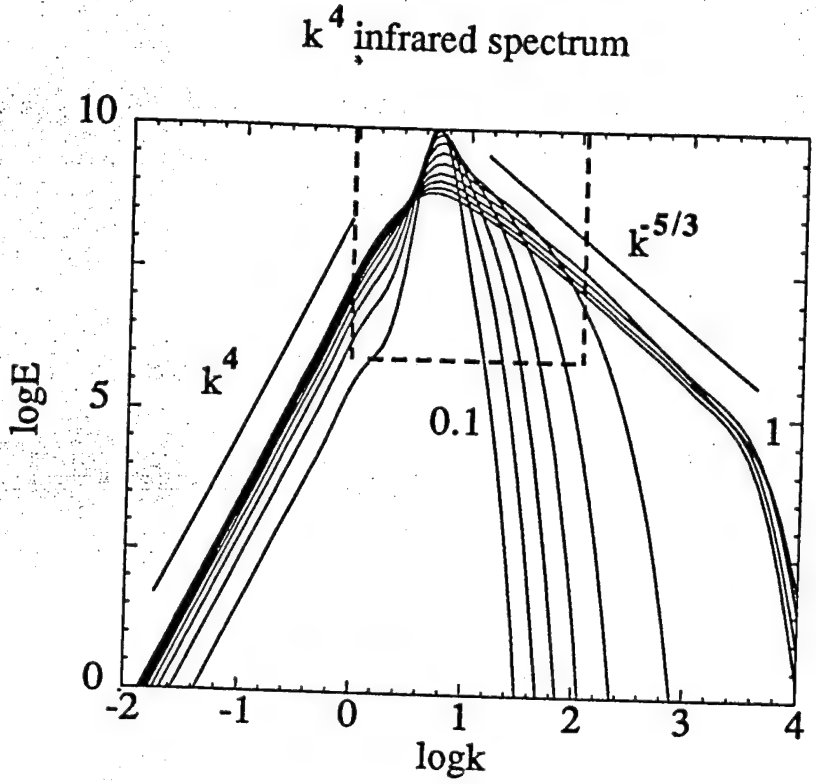

Figure 2 (a)

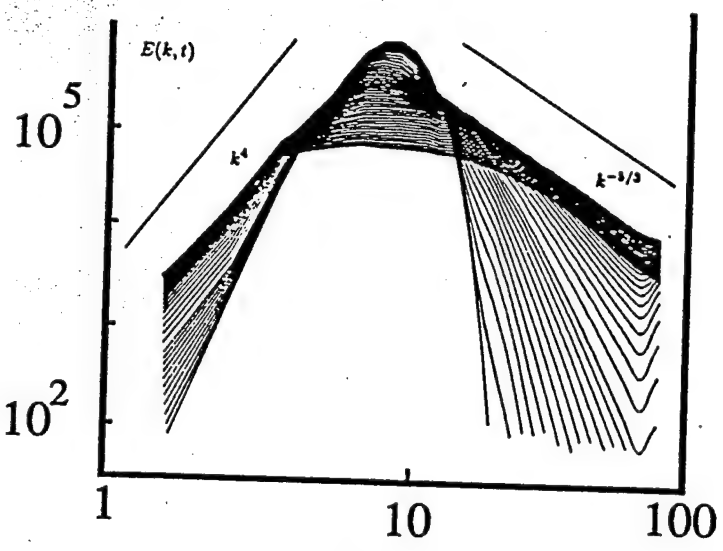

Figure 2(b)

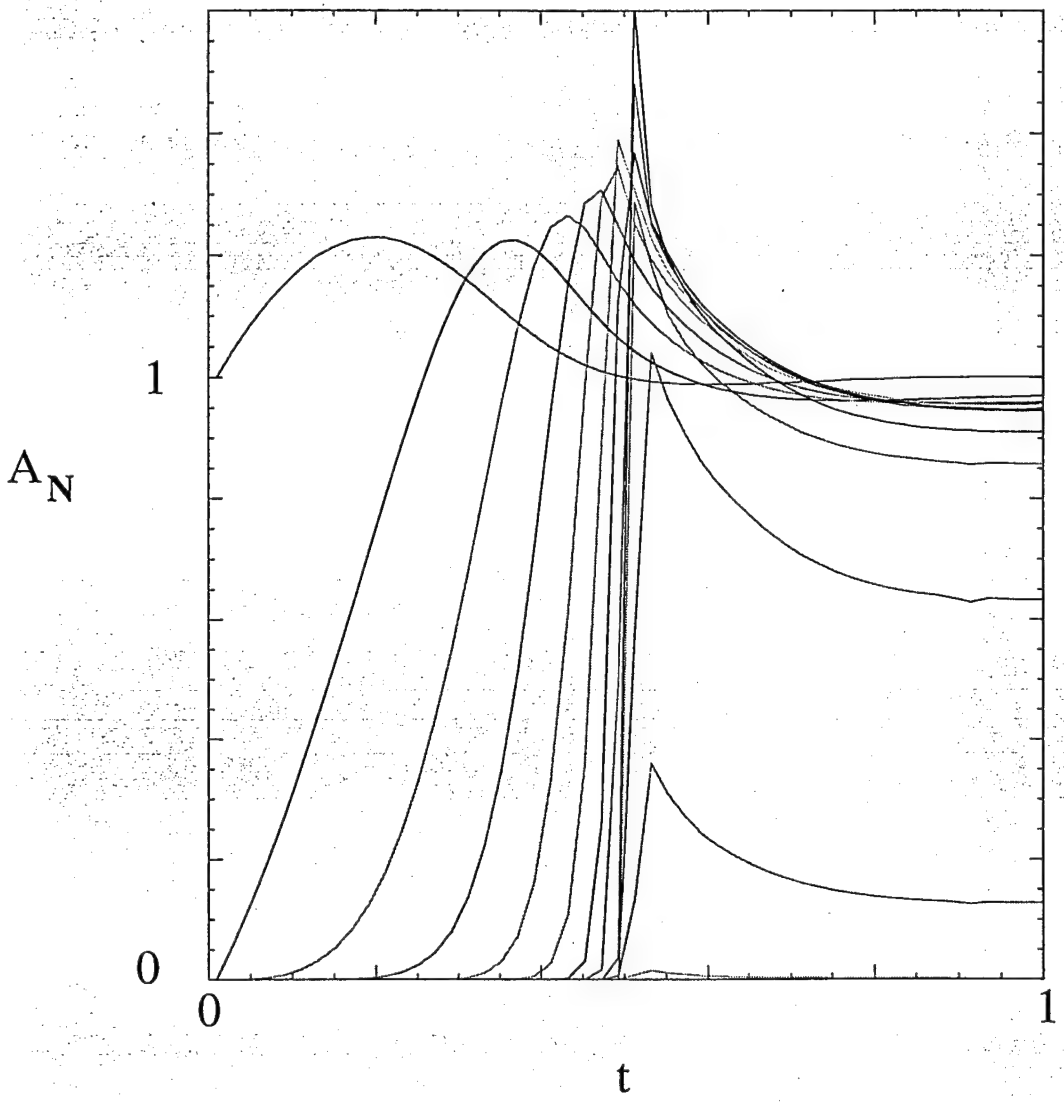

Figure 3

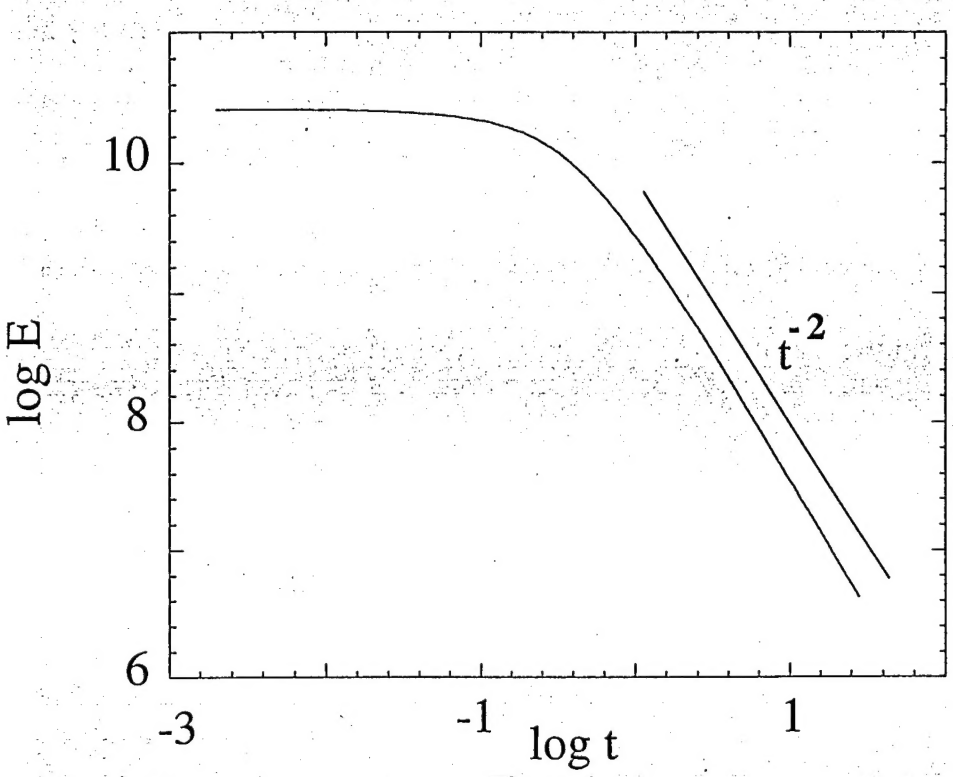

Figure 4

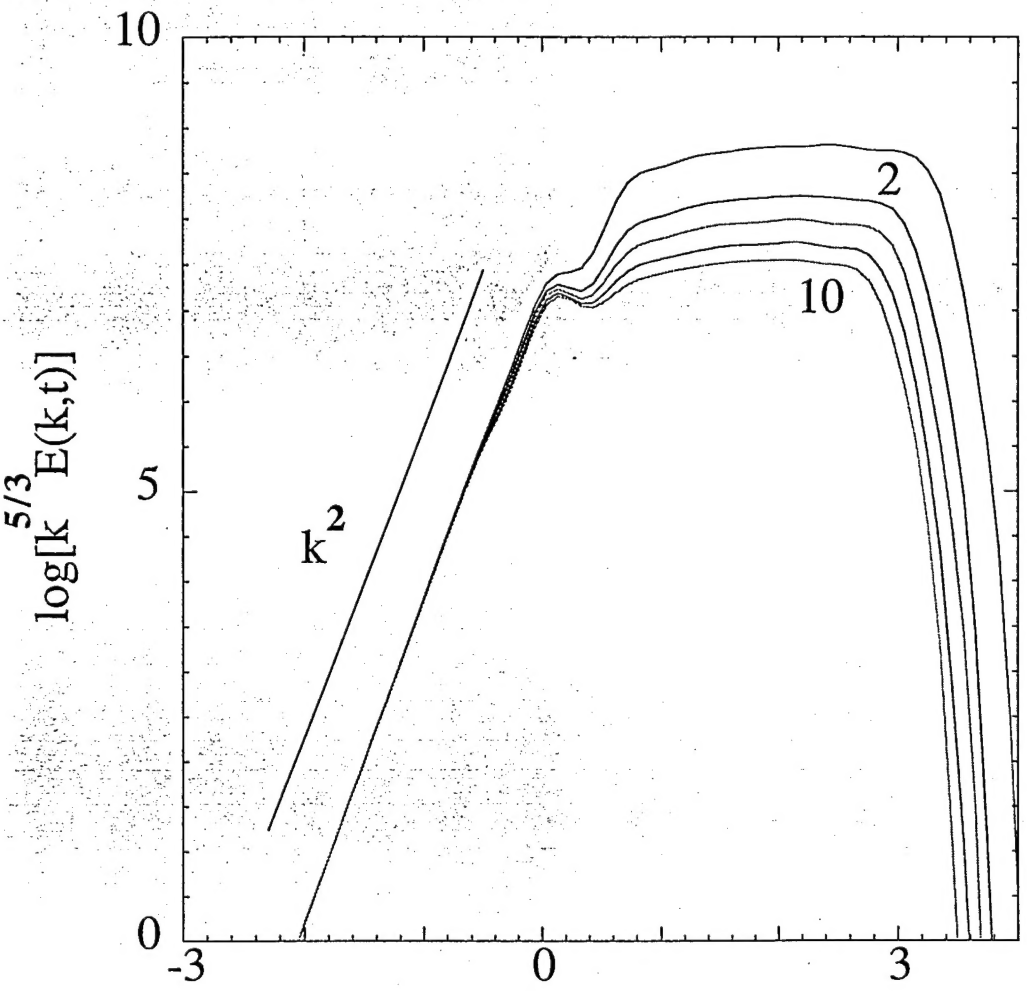

Figure 5

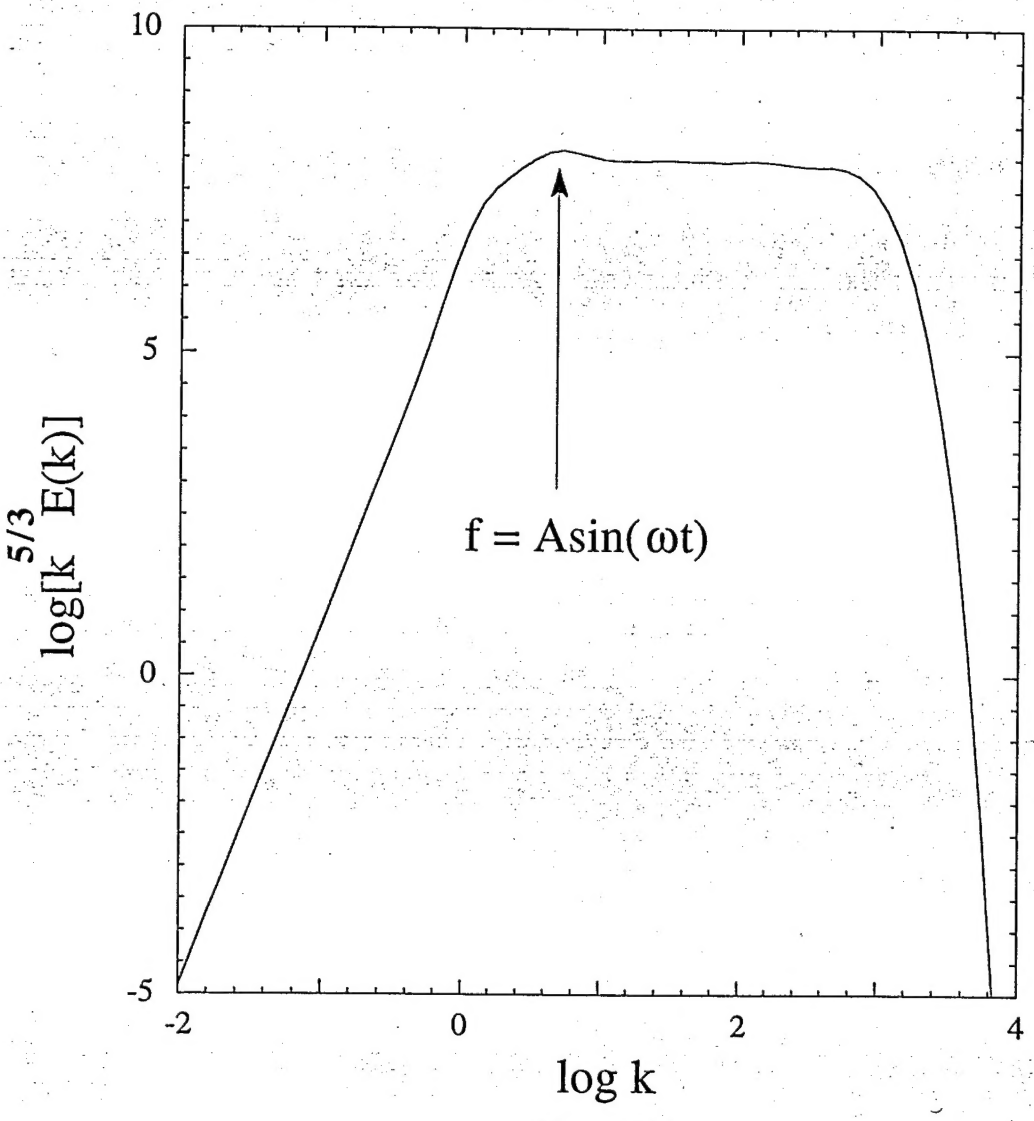

Figure 6(a)

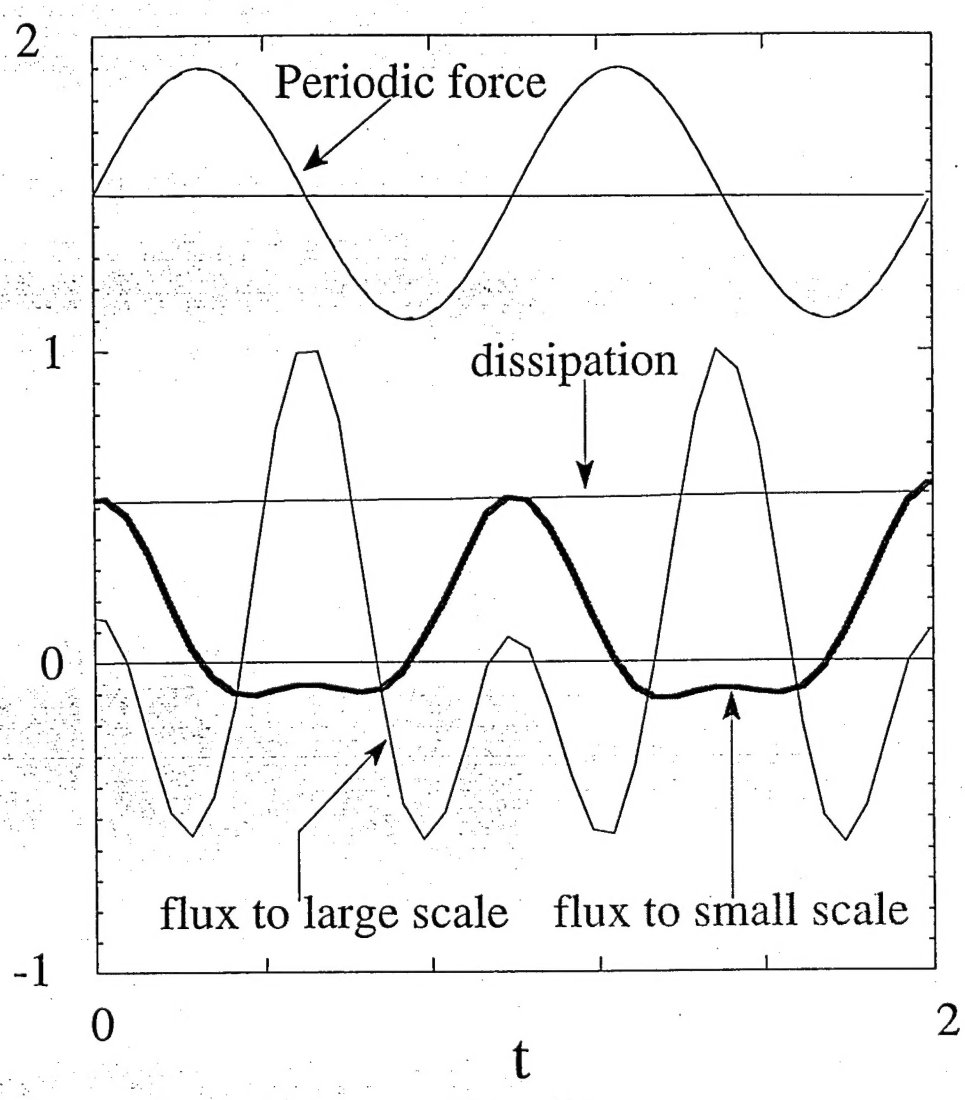
2
1
0
-1
0
2
t
Periodic force
dissipation
flux to large scale
flux to small scale

Figure 6(b)